Electronic Supplementary Information

Optimization of Aggregation-Induced Phosphorescence Emission in Mononuclear Tricarbonyl Rhenium(I) Complexes: The Influence of Steric Hindrance and Isomerism

Jinhui Wang, Alexandre Poirot, Béatrice Delavaux-Nicot, Mariusz Wolff, Sonia Mallet-Ladeira, Jan Patrick Calupitan, Clémence Allain, Eric Benoist and Suzanne Fery-Forgues *

List of Tables

List of Figures

Tables

Table S1. Selected bond lengths (Å) for both molecules of the asymmetric unit of **ReL3** and for **ReL4**. The atoms were numbered like on the molecular views. For the sake of comparison, each line corresponds to the same bond in both complexes.

Bond lengths	ReL3	Bond lengths	ReL4
Re(1)-C(2) / Re(2)-C(27)	1.94(2) / 1.89(2)	Re(1)-C(1)	1.90(1)
Re(1)-C(1) / Re(2)-C(28)	1.92(2) / 1.95(2)	Re(1)-C(2)	1.92(1)
Re(1)-C(200) / Re(2)-C(400)	2.02(5) / 2.04(4)	Re(1)-C(3)	1.90(1)
Re(1)-N(1) / Re(2)-N(6)	2.146(11) / 2.216(16)	Re(1)-N(1)	2.198(4)
Re(1)-N(2) / Re(2)-N(7)	2.122(13) / 2.126(12)	Re(1)-N(2)	2.155(5)
Re(1)-Cl(2) / Re(2)-Cl(4)	2.425(14) / 2.433(15)	Re(1)-Cl(1)	2.488(2)
C(2)-O(2) / C(27)-O(4)	1.13(2) / 1.20(2)	C(1)-O(1)	1.16(1)
C(1)-O(1) / C(28)-O(5)	1.13(2) / 1.14(2)	C(2)-O(2)	1.15(1)
C(200)-O(200) / C(400)-O(400)	1.13(6) / 1.15(5)	C(3)-O(3)	1.15(1)

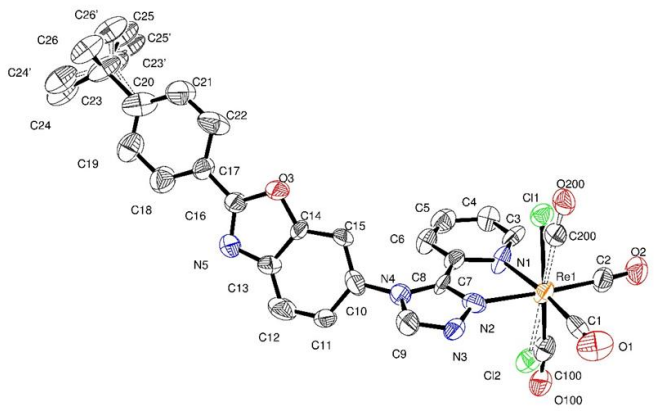

ReL3

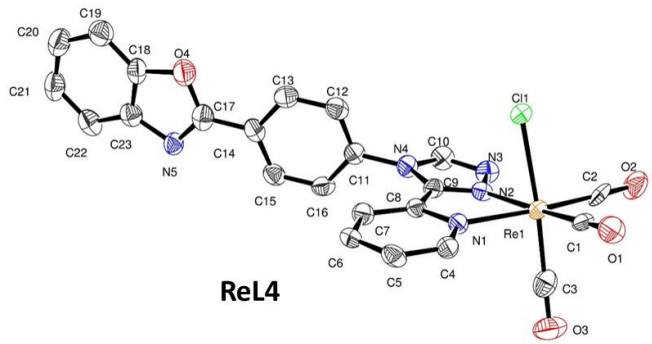

ReL4

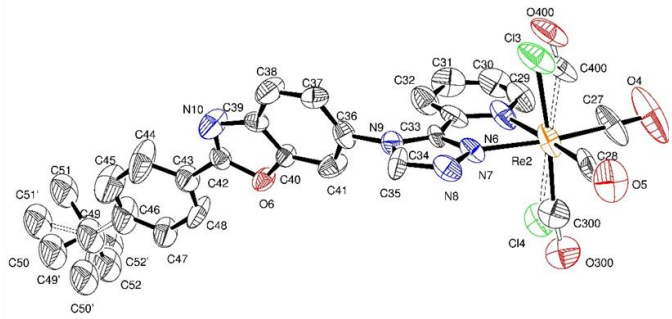

Table S2. Selected angles (°) for both molecules of the asymmetric unit of **ReL3** and for **ReL4**. The atoms were numbered like on the molecular views. For the sake of comparison, each line corresponds to the same angle in both complexes.

Bond angles	**ReL3**	Bond angles	**ReL4**
C(2)-Re(1)-C(1)/C(27)-Re(2)-C(28)	87.1(7)/ 87.5(9)	C(1)-Re(1)-C(2)	89.7(2)
C(2)-Re(1)-C(200)/C(27)-Re(2)-C400)	86.3(13)/ 78.8(19)/	C(1)-Re(1)-C(3)	87.2(3)
C(1)-Re(1)-C(200)/C(28)-Re(2)-C400)	86.3(13)/ 90(2)	C(2)-Re(1)-C(3)	91.0(3)
C(2)-Re(1)-N(2)/C(27)-Re(2)-N(7)	173.0(6)/ 170.6(8)	C(1)-Re(1)-N(2)	170.8(2)
C(1)-Re(1)-N(2)/C(28)-Re(2)-N(7)	99.7(6)/ 101.6(5)	C(2)-Re(1)-N(2)	97.5(2)
C(200)-Re(1)-N(2)/C(400)-Re(2)-N(7)	95.5(13)/ 98.7(18)	C(3)-Re(1)-N(2)	98.4(2)
C(2)-Re(1)-N(1)/C(27)-Re(2)-N(6)	99.4(6)/ 97.4(9)	C(1)-Re(1)-N(1)	98.2(2)
C(1)-Re(1)-N(1)/C(28)-Re(2)-N(6)	172.9(5)/ 175.0(6)	C(2)-Re(1)-N(1)	172.0(2)
C(200)-Re(1)-N(1)/C(400)-Re(2)-N(6)	96.8(13)/ 90(2)	C(3)-Re(1)-N(1)	90.9(3)
N(2)-Re(1)-N(1)/N(7)-Re(2)-N(6)	73.7(5)/ 73.5(5)	N(2)-Re(1)-N(1)	74.5(2)
C(2)-Re(1)-Cl(2)/C(27)-Re(2)-Cl(4)	96.1(7)/ 95.9(8)	C(1)-Re(1)-Cl(1)	92.6(2)
C(1)-Re(1)-Cl(2)/C(28)-Re(2)-Cl(4)	91.9(6)/ 97.5(6)	C(2)-Re(1)-Cl(1)	94.1(2)
C(200)-Re(1)-Cl(2)/C(400)-Re(2)-Cl(4)	176.9(12)/ 171.1(19)	C(3)-Re(1)-Cl(1)	175.0(2)
N(2)-Re(1)-Cl(2)/N(7)-Re(2)-Cl(4)	82.4(5)/ 85.4(5)	N(2)-Re(1)-Cl(1)	81.2(1)
N(1)-Re(1)-Cl(2)/N(6)-Re(2)-Cl(4)	84.7(5)/ 83.3(5)	N(1)-Re(1)-Cl(1)	84.2(1)
O(2)-C(2)-Re(1)/O(4)-C(27)-Re(2)	177.0(16)/ 178(3)	O(1)-C(1)-Re(1)	179.4(6)
O(1)-C(1)-Re(1)/O(5)-C(28)-Re(2)	169.9(17)/ 178.8(18)	O(2)-C(2)-Re(1)	178.9(6)
O(200)-C(200)-Re(1)/O(400)-C(400)-Re(2)	178(4)/ 151(5)	O(3)-C(3)-Re(1)	175.8(6)

Table S3. Comparison between experimental and theoretical selected bond lengths (Å) and angles (°) for **ReL3** in CH_2Cl_2.

Bond lengths	**Exp.**	**Optimized**			**Bond angles**	**Exp.**	**Optimized**		
		S_0	**S_1**	**T_1**			**S_0**	**S_1**	**T_1**
Re(1)-C(1)	1.92(2)	1.916	*1.958*	*1.986*	C(1)-Re(1)-C(2)	87.1(7)	89.69	*85.18*	*88.40*
Re(1)-C(2)	1.941(19)	1.912	*1.949*	*1.933*	C(1)-Re(1)-C(100)	86.7(17)	90.57	*90.32*	*89.24*
Re(1)-C(100)	1.97(6)	1.896	*1.954*	*1.950*	C(2)-Re(1)-C(100)	85.8(17)	90.37	*93.63*	*92.49*
Re(1)-N(1)	2.122(13)	2.212	*2.153*	*2.164*	C(1)-Re(1)-N(1)	99.7(6)	98.45	*100.54*	*98.78*
Re(1)-N(2)	2.146(11)	2.146	*2.097*	*2.042*	C(2)-Re(1)-N(1)	173.0(6)	170.73	*173.86*	*171.82*
Re(1)-Cl(1)	2.473(11)	2.524	*2.421*	*2.455*	C(100)-Re(1)-N(1)	93.1(16)	93.95	*88.61*	*91.52*
					C(1)-Re(1)-N(2)	172.9(5)	171.38	*176.45*	*175.29*
C(1)-O(1)	1.13(2)	1.160	*1.151*	*1.148*	C(2)-Re(1)-N(2)	99.4(6)	97.58	*98.11*	*96.31*
C(2)-O(2)	1.125(19)	1.158	*1.150*	*1.153*	C(100)-Re(1)-N(2)	91.0(17)	94.01	*90.81*	*90.41*
C(100)-O(100)	1.16(8)	1.164	*1.148*	*1.149*	N(1)-Re(1)-N(2)	73.7(5)	73.96	*76.13*	*76.52*
					C(1)-Re(1)-Cl(1)	97.8(6)	91.56	*90.51*	*86.97*
					C(2)-Re(1)-Cl(1)	92.4(6)	92.32	*91.82*	*91.68*
					C(100)-Re(1)-Cl(1)	175.1(17)	176.58	*174.54*	*174.28*
					N(1)-Re(1)-Cl(1)	88.0(4)	83.09	*85.93*	*84.83*
					N(2)-Re(1)-Cl(1)	84.7(5)	83.55	*88.05*	*93.01*
					Re(1)-C(1)-O(1)	169.9(17)	179.30	*178.59*	*179.07*
					Re(1)-C(2)-O(2)	177.0(16)	178.81	*179.89*	*179.03*
					Re(1)-C(100)-O(100)	171(5)	179.83	*179.14*	*179.49*

Table S4. Comparison between experimental and theoretical selected bond lengths (Å) and angles (°) for **ReL4** in CH_2Cl_2.

Bond lengths	**Exp.**	**Optimized**			**Bond angles**	**Exp.**	**Optimized**		
		S_0	**S_1**	**T_1**			**S_0**	**S_1**	**T_1**
Re(1)-C(1)	1.902(7)	1.916	*1.957*	*1.988*	C(1)-Re(1)-C(2)	89.7(2)	89.69	*85.14*	*88.55*
Re(1)-C(2)	1.920(7)	1.913	*1.949*	*1.932*	C(1)-Re(1)-C(3)	87.2(3)	90.57	*90.42*	*89.15*
Re(1)-C(3)	1.903(8)	1.897	*1.955*	*1.951*	C(2)-Re(1)-C(3)	91.0(3)	90.35	*93.52*	*92.23*
Re(1)-N(1)	2.198(4)	2.212	*2.155*	*2.169*	C(1)-Re(1)-N(1)	98.2(2)	98.47	*100.61*	*98.77*
Re(1)-N(2)	2.155(5)	2.146	*2.097*	*2.041*	C(2)-Re(1)-N(1)	172.0(2)	171.34	*173.88*	*171.72*
Re(1)-Cl(1)	2.4882(15)	2.524	*2.419*	*2.451*	C(3)-Re(1)-N(1)	90.9(3)	93.96	*88.56*	*91.74*
					C(1)-Re(1)-N(2)	170.8(2)	171.34	*176.37*	*175.13*
C(1)-O(1)	1.160(7)	1.916	*1.150*	*1.148*	C(2)-Re(1)-N(2)	97.5(2)	97.56	*98.19*	*96.31*
C(2)-O(2)	1.148(7)	1.913	*1.150*	*1.153*	C(3)-Re(1)-N(2)	98.4(2)	94.09	*90.83*	*90.37*
C(3)-O(3)	1.151(8)	1.897	*1.148*	*1.149*	N(1)-Re(1)-N(2)	74.49(18)	73.96	*76.01*	*76.40*
					C(1)-Re(1)-Cl(1)	92.64(18)	91.50	*90.52*	*86.87*
					C(2)-Re(1)-Cl(1)	94.06(19)	92.50	*91.92*	*91.74*
					C(3)-Re(1)-Cl(1)	175.0(2)	176.49	*174.54*	*174.30*
					N(1)-Re(1)-Cl(1)	84.20(13)	82.93	*85.98*	*84.85*
					N(2)-Re(1)-Cl(1)	81.15(13)	83.50	*87.92*	*93.25*
					Re(1)-C(1)-O(1)	179.4(6)	179.27	*178.65*	*179.14*
					Re(1)-C(2)-O(2)	178.9(6)	178.80	*179.86*	*178.96*
					Re(1)-C(3)-O(3)	175.8(6)	179.81	*179.17*	*179.55*

Table S5. Composition of the frontier molecular orbitals (%) and energy levels in CH_2Cl_2 for complexes **ReL3** and **ReL4**.

Orbital		**Energy (eV)**	**MO Contribution (%)**					**Main bond type**
			Re	**CO**	**Cl**	**Pyta**	**PBO**	
ReL3 (GAP = 4.07 eV)								
142	LUMO+5	–0.71	30	44	0	0	28	p(Re) + π*(CO) + π*(PBO)
141	LUMO+4	–0.81	21	43	0	6	30	p(Re) + π*(CO) + π*(PBO)
140	LUMO+3	–0.85	12	19	0	13	56	π*(PBO) + π*(Pyta)
139	LUMO+2	–1.63	0	1	0	95	4	π*(Pyta)
138	LUMO+1	–2.05	0	0	0	2	97	π*(PBO)
137	LUMO	–2.52	3	4	1	91	2	π*(Pyta)
136	HOMO	–6.59	52	24	19	4	0	d(Re) + π(CO) + p(Cl)
135	HOMO–1	–6.71	52	22	22	4	0	d(Re) + π(CO) + p(Cl)
134	HOMO–2	–6.87	0	0	0	2	98	π(PBO)
133	HOMO–3	–7.15	69	30	1	0	0	d(Re) + π(CO)
132	HOMO–4	–7.66	0	0	0	0	100	π(PBO)
131	HOMO–5	–7.81	2	0	28	68	2	π(Pyta) + π(Cl)
ReL4 (GAP = 4.06 eV)								
126	LUMO+5	–0.72	37	57	0	1	6	p(Re) + π*(CO)
125	LUMO+4	–0.83	34	59	0	7	0	p(Re) + π*(CO)
124	LUMO+3	–1.14	0	0	0	12	87	π*(PBO) + π*(Pyta)
123	LUMO+2	–1.66	0	1	0	92	7	π*(Pyta)
122	LUMO+1	–2.23	0	0	0	3	97	π*(PBO)
121	LUMO	–2.54	3	4	1	91	2	π*(Pyta)
120	HOMO	–6.60	52	24	20	4	0	d(Re) + π(CO) + p(Cl)
119	HOMO–1	–6.72	52	22	22	5	0	d(Re) + π(CO) + p(Cl)
118	HOMO–2	–6.93	0	0	0	1	99	π(PBO)
117	HOMO–3	–7.16	69	30	1	0	0	d(Re) + π(CO)
116	HOMO–4	–7.44	0	0	0	0	100	π(PBO)
115	HOMO–5	–7.82	2	0	29	69	0	π(Pyta) + π(Cl)

Pyta: pyridyltriazole, PBO: 2-phenylbenzoxazole

Table S6. Main electronic transitions for complex **ReL3** in CH_2Cl_2 calculated with TDDFT method at the PBE1PBE/LANL2DZ level.

Electronic transition	Contribution	Assignment		E_{calc}/eV	λ_{calc}/nm	*f*
$S_0 \rightarrow S_1$	HOMO → LUMO	d(Re) + π(CO) + p(Cl) → π*(Pyta)	MLCT/LLCT	3.07	403.6	*0.0012*
$S_0 \rightarrow S_2$	H – 1 → LUMO	d(Re) + π(CO) + p(Cl) → π*(Pyta)	MLCT/LLCT	3.28	378.3	*0.1294*
$S_0 \rightarrow S_6$	H – 2 → L + 1	π(PBO) → π*(PBO)	ILCT	4.12	300.8	*1.2509*
$S_0 \rightarrow S_7$	HOMO → L + 1	d(Re) + π(CO) + p(Cl) → π*(PBO)	LMCT/LLCT	4.17	297.5	*0.1004*
	HOMO → L + 2	d(Re) + π(CO) + p(Cl) → π*(Pyta)	LMCT/LLCT			
$S_0 \rightarrow S_{12}$	H – 5 → LUMO	π(Pyta) + π(Cl) → π*(Pyta)	ILCT/LLCT	4.44	279.5	*0.1690*
$S_0 \rightarrow S_{16}$	H – 7 → LUMO	π(Cl) → π*(Pyta)	LLCT	4.66	266.2	*0.0343*
$S_0 \rightarrow S_{22}$	H – 9 → LUMO	π(Cl) + π(Pyta) → π*(Pyta)	LLCT/ILCT	4.86	255.2	*0.1182*
$S_0 \rightarrow S_{24}$	H – 6 → L + 1	π(PBO) → π*(PBO)	ILCT	4.94	251.1	*0.0346*
$S_0 \rightarrow S_{25}$	H – 3 → L + 4	d(Re) + π(CO) →p(Re)+π*(CO)+π*(PBO)		5.08	244.2	*0.0452*
$S_0 \rightarrow S_{30}$	H – 5 → L + 2	π(Pyta) + π(Cl) → π*(Pyta)	ILCT/LLCT	5.35	231.8	*0.1204*
$S_0 \rightarrow S_{31}$	H – 2 → L + 3	π(PBO) → π*(PBO) + π*(Pyta)	ILCT/LLCT	5.36	231.3	*0.0440*
$S_0 \rightarrow S_{42}$	H – 7 → L + 2	π(Cl) → π*(Pyta)	LLCT	5.60	221.3	*0.0368*
	H – 7 → L + 1	π(Cl) → π*(PBO)	LLCT			
$S_0 \rightarrow S_{50}$	H – 2 → L + 7	π(PBO) → π*(PBO)	ILCT	5.76	215.3	*0.0948*
$S_0 \rightarrow S_{72}$	H – 5 → L + 5	π(Pyta) + π(Cl) →p(Re)+π*(CO) +π*(PBO)	LMCT/LLCT	6.18	200.5	*0.1067*

MLCT: metal-to-ligand charge transfer; LMCT: ligand-to-metal charge transfer; LLCT: ligand-to-ligand charge transfer; ILCT: intraligand charge transfer.

Table S7. Main electronic transitions for complex **ReL4** in CH_2Cl_2 calculated with TDDFT method at the PBE1PBE/LANL2DZ level.

Electronic transition	Contribution	Assignment		E_{calc}/eV	λ_{calc}/nm	*f*
$S_0 \rightarrow S_1$	HOMO → LUMO	d(Re) + π(CO) + p(Cl) → π*(Pyta)	MLCT/LLCT	3.06	404.7	*0.0012*
$S_0 \rightarrow S_2$	H – 1 → LUMO	d(Re) + π(CO) + p(Cl) → π*(Pyta)	MLCT/LLCT	3.27	379.2	*0.1323*
$S_0 \rightarrow S_4$	H – 2 → LUMO	π(PBO) → π*(Pyta)	LLCT	3.90	317.9	*0.0331*
$S_0 \rightarrow S_7$	H – 2 → L + 1	π(PBO) → π*(PBO)	ILCT	4.03	307.3	*1.0069*
$S_0 \rightarrow S_{12}$	H – 5 → LUMO	π(Pyta) + π(Cl) → π*(Pyta)	ILCT/LLCT	4.43	279.8	*0.1628*
$S_0 \rightarrow S_{18}$	H – 6 → LUMO	π(Cl) + π(Pyta) → π*(Pyta)	LLCT/ILCT	4.64	267.1	*0.0393*
$S_0 \rightarrow S_{21}$	H – 7 → LUMO	π(PBO) + π(Pyta) + π(Cl) → π*(Pyta)	LLCT/ILCT	4.84	256.1	*0.1282*
	H – 8 → LUMO	π(PBO) + π(Cl) + π(Pyta) → π*(Pyta)	LLCT/ILCT			
$S_0 \rightarrow S_{28}$	H – 3 → L + 4	d(Re) + π(CO) → p(Re) + π*(CO)	MLCT/ILCT	5.10	243.3	*0.0625*
$S_0 \rightarrow S_{30}$	H – 5 → L + 2	π(Pyta) + π(Cl) → π*(Pyta)	ILCT/LLCT	5.32	232.9	*0.1095*
$S_0 \rightarrow S_{33}$	H – 4 → L + 2	π(PBO) → π*(Pyta)	LLCT	5.39	229.9	*0.0326*
$S_0 \rightarrow S_{36}$	H – 10 → LUMO	π(Cl) → π*(Pyta)	LLCT	5.45	227.4	*0.0340*
$S_0 \rightarrow S_{37}$	H – 2 → L + 6	π(PBO) → π*(PBO)	ILCT	5.46	227.1	*0.0361*
$S_0 \rightarrow S_{39}$	H – 8 → L + 1	π(PBO) + π(Cl) + π(Pyta) → π*(PBO)	ILCT/LLCT	5.49	225.7	*0.0409*
$S_0 \rightarrow S_{42}$	H – 9 → L + 1	π(PBO) + π(Pyta) → π*(PBO)	ILCT/LLCT	5.60	221.2	*0.1271*
$S_0 \rightarrow S_{43}$	H – 6 → L + 2	π(Cl) + π(Pyta) → π*(Pyta)	LLCT/ILCT	5.62	220.6	*0.1087*
$S_0 \rightarrow S_{55}$	H – 3 → L + 10	d(Re) + π(CO) → π*(CO) + π*(Pyta)	MLCT/LLCT	5.87	211.1	*0.0347*
$S_0 \rightarrow S_{56}$	H – 8 → L + 2	π(PBO) + π(Cl) + π(Pyta) → π*(Pyta)	LLCT/ILCT	5.90	210.3	*0.0812*
	H – 7 → L + 2	π(PBO) + π(Pyta) + π(Cl) → π*(Pyta)	LLCT/ILCT			
$S_0 \rightarrow S_{69}$	H – 13 → LUMO	π(Pyta) → π*(Pyta)	ILCT	6.16	201.2	*0.0560*

MLCT: metal-to-ligand charge transfer; LMCT: ligand-to-metal charge transfer; LLCT: ligand-to-ligand charge transfer; ILCT: intraligand charge transfer.

Table S8. Four calculated singlet states for complexes **ReL3** and **ReL4** in S_1 optimized geometry calculated with TDDFT method at PBE1PBE/LANL2DZ level.

ReL3

State	Contribution	Assignment		E_{calc} /eV	λ_{calc} /nm	*f*
1	HOMO → LUMO	d(Re) + π(CO) + p(Cl) → π*(Pyta)	MLCT/LLCT	2.29	540.4	*0.0025*
2	H – 1 → LUMO	d(Re) + π(CO) + p(Cl) → π*(Pyta)	MLCT/LLCT	2.70	458.8	*0.1929*
3	H – 3 → LUMO	d(Re) + π(CO) + π(PBO) → π*(Pyta)	MLCT/LLCT	2.99	415.2	*0.0002*
4	H – 2 → LUMO	π(PBO) + d(Re) + π(CO) → π*(Pyta)	LLCT/MLCT	3.45	359.1	*0.1404*

ReL4

State	Contribution	Assignment		E_{calc} /eV	λ_{calc} /nm	*f*
1	HOMO → LUMO	d(Re) + π(CO) + p(Cl) → π*(Pyta)	MLCT/LLCT	2.25	550.8	*0.0042*
2	H – 1 → LUMO	d(Re) + π(CO) + p(Cl) → π*(Pyta)	MLCT/LLCT	2.65	467.1	*0.2147*
3	H – 3 → LUMO	d(Re) + π(CO) + π(PBO) → π*(Pyta)	MLCT/LLCT	2.94	421.0	*0.0008*
4	HOMO → L + 1	d(Re) + π(CO) + p(Cl) → π*(PBO)	MLCT/LLCT	3.42	363.1	*0.3532*
	H – 2 → LUMO	π(PBO) + d(Re) + π(CO) → π*(Pyta)	LLCT/MLCT			

Molecular orbital characters in S_0 geometry are different than in S_1 geometry or T_1 geometry.

Table S9. Calculated phosphorescence emission energies of **ReL3** and **ReL4**, in comparison to the experimental values recorded in CH_2Cl_2.

Cpd	DFT		TD-DFT				λ_{exp} (nm)
	ΔE_{T1-S0} (eV/nm)	Character	Major contribution (C_i coefficient)	E (eV)	λ_{cal} (nm)	Character	
ReL3	2.04/607.8	^{3}MLCT/^{3}LLCT/^{3}IL	L → H (0.675)	1.93	642.8	^{3}MLCT/^{3}LLCT d(Re)+π(CO)+p(Cl)→π*(Pyta)	627
ReL4	1.98/626.2	^{3}MLCT/^{3}LLCT/^{3}IL	L → H (0.672)	1.88	658.6	^{3}MLCT/^{3}LLCT d(Re)+π(CO)+p(Cl)→π*(Pyta)	632

ΔE_{T1-S0} is the energy difference between the ground singlet and triplet states.

Table S10. Occupancy and hybridization of the calculated natural bond orbitals (NBOs) between the rhenium and the carbonyl ligands for complexes **ReL3** and **ReL4**.

ReL3

Bond	Occupancy	Hybridization of NBO		
Re(1)–C(1)	1.965 (0.206)	0.6177 $(sp^{0.67}d^{2.56})_{Re}$ + 0.7864 $(sp^{0.52})_C$	38.16%	61.84%
Re(1)–C(2)	1.966 (0.200)	0.6211 $(sp^{0.63}d^{2.59})_{Re}$ + 0.7838 $(sp^{0.53})_C$	38.57%	61.43%
Re(1)–C(3)	1.919 (0.102)	0.5969 $(sp^{2.89}d^{3.14})_{Re}$ + 0.8023 $(sp^{0.53})_C$	35.63%	64.37%
C(1)–O(1)	1.997 (0.016)	0.5583 $(sp^{1.90})_C$ + 0.8297 $(sp^{1.20})_O$	31.16%	68.84%
	1.996 (0.219)	0.4905 $(p)_C$ + 0.8715 $(p)_O$	24.06%	75.94%
	1.995 (0.194)	0.4953 $(p)_C$ + 0.8687 $(p)_O$	24.53%	75.47%
C(2)–O(2)	1.997 (0.025)	0.5558 $(sp^{1.98})_C$ + 0.8313 $(sp^{1.31})_O$	30.89%	69.11%
	1.996 (0.208)	0.4915 $(p)_C$ + 0.8709 $(p)_O$	24.16%	75.84%
	1.995 (0.182)	0.4979 $(p)_C$ + 0.8672 $(p)_O$	24.79%	75.21%
C(3)–O(3)	1.997 (0.023)	0.5583 $(sp^{1.90})_C$ + 0.8296 $(sp^{1.20})_O$	31.17%	68.83%
	1.997 (0.246)	0.4879 $(p)_C$ + 0.8729 $(p)_O$	23.80%	76.20%
	1.995 (0.210)	0.4966 $(p)_C$ + 0.8680 $(p)_O$	24.66%	75.34%

ReL4

Bond	Occupancy	Hybridization of NBO		
Re(1)–C(1)	1.965 (0.206)	0.6178 $(sp^{0.67}d^{2.56})_{Re}$ + 0.7864 $(sp^{0.52})_C$	38.16%	61.84%
Re(1)–C(2)	1.966 (0.200)	0.6210 $(sp^{0.63}d^{2.58})_{Re}$ + 0.7838 $(sp^{0.53})_C$	38.57%	61.43%
Re(1)–C(3)	1.920 (0.103)	0.5970 $(sp^{2.89}d^{3.15})_{Re}$ + 0.8022 $(sp^{0.53})_C$	35.64%	64.36%
C(1)–O(1)	1.997 (0.016)	0.5582 $(sp^{1.90})_C$ + 0.8297 $(sp^{1.20})_O$	31.16%	68.84%
	1.996 (0.219)	0.4905 $(p)_C$ + 0.8714 $(p)_O$	24.06%	75.94%
	1.995 (0.194)	0.4954 $(p)_C$ + 0.8687 $(p)_O$	24.54%	75.46%
C(2)–O(2)	1.997 (0.025)	0.5558 $(sp^{1.98})_C$ + 0.8313 $(sp^{1.31})_O$	30.89%	69.11%
	1.996 (0.208)	0.4916 $(p)_C$ + 0.8708 $(p)_O$	24.16%	75.84%
	1.995 (0.182)	0.4980 $(p)_C$ + 0.8672 $(p)_O$	24.80%	75.20%
C(3)–O(3)	1.997 (0.024)	0.5582 $(sp^{1.96})_C$ + 0.8297 $(sp^{1.30})_O$	31.16%	68.84%
	1.997 (0.245)	0.4879 $(p)_C$ + 0.8729 $(p)_O$	23.81%	76.19%
	1.995 (0.210)	0.4968 $(p)_C$ + 0.8679 $(p)_O$	24.68%	75.32%

Table S11. Atomic charges from the Natural Population Analysis (NPA) for **ReL3** and **ReL4**.

Atom	Charge	
	ReL3	**ReL4**
Re(1)	–0.99	–0.99
C(1)	+0.76	+0.76
C(2)	+0.78	+0.78
C(3)	+0.74	+0.74
O(1)	–0.48	–0.48
O(2)	–0.48	–0.48
O(3)	–0.50	–0.50
N(1)	–0.39	–0.38
N(2)	–0.23	–0.23
Cl(1)	–0.46	–0.46

Table S12. Natural populations of the $5d_{xy}$, $5d_{xz}$, $5d_{yz}$, $5d_{x^2-y^2}$ and $5d_{z^2}$ orbitals of the central atom in **ReL3** and **ReL4**.

Orbital	Natural population	
	ReL3	**ReL4**
$\mathbf{d_{xy}}$	1.149	1.007
$\mathbf{d_{xz}}$	1.219	1.496
$\mathbf{d_{yz}}$	1.327	1.557
$\mathbf{d_{x^2-y^2}}$	1.519	1.538
$\mathbf{d_{z^2}}$	1.471	1.087

Table S13. Absolute electronegativity, absolute hardness, dipole moment (μ), electrophilicity index (ω) and global softness (σ) of complexes **ReL3** and **ReL4** in CH_2Cl_2.

Parameters	Complex	
	ReL3	**ReL4**
E_{HOMO} (eV)	–6.59	–6.60
E_{LUMO} (eV)	–2.52	–2.54
Energy gap ΔE (eV)	4.07	4.06
Electronegativity μ (eV)	4.56	4.57
Hardness η (eV)	2.04	2.03
Dipole moment μ (Debye)	20.86	19.76
Electrophilicity ω (eV)	5.10	5.14
Softness σ (1/eV)	0.49	0.49

Table S14. Selected electrochemical data of ligands **L3**, **L4** [1.0×10^{-3} M] , and complexes **ReL3**, **ReL4** [6.5×10^{-4} M]. Values determined by OSWV on a Pt working electrode in CH_2Cl_2 + 0.1 M *n*-Bu_4NBF_4 at room temperature.[a,b] Ferrocene was used as internal reference**.**

	Oxidation		Reduction		
	E_2	E_1	E_1	E_2	E_3
L1	---	---	–1.96	---	
L3	---	1.72[c]	–1.53[e]	–2.05	
L4	---	2.07	–1.84	–2.20	
ReL1	1.74	1.44	–1.31[d]	–1.90	
ReL3	1.75	1.44	–1.32[d]	–2.02	
ReL4	1.73	1.44	–1.28[f]	–1.58	–1.83[g]

[a] OSWVs were obtained using a sweep width of 20 mV, a frequency of 20 Hz, and a step potential of 5 mV.
[b] Potential values in Volts vs. SCE (Fc^+/Fc is observed at 0.55 V ± 0.01 V *vs.* SCE). **L1** and **ReL1** data from ref.[8] [c] Very broad peak, not well-distinguishable. [d] quasi-reversible at 1 V/s. [e] Minor intensity, becomes quasi-reversible around 20 V/s. [f] Quasi-reversible process at 0.2 V/s. [g] With a shoulder at the right side.

Table S15. Experimental electrochemical data used, and calculated values of the energy gaps (E_g) for compounds **ReL3** and **ReL4**.

Compound	E_{onset} ox (V)	E_{onset} red (V)	E_{HOMO} (eV)	E_{LUMO} (eV)	E_g^{el} (eV)	E_{calc}* (eV)	λ_{calc}* (nm)
ReL3	1.34	–1.21	–6.08	–3.53	2.55	2.70	458.8
ReL4	1.34	–1.16	–6.08	–3.58	2.50	2.65	467.1

*Values obtained from theoretical study, see Table S8.

Evaluation of the energy gap values (E_g) for the Re complexes.

The onset oxidation and reduction potentials (E_{onset} ox, E_{onset} red) were measured by cyclic voltammetry in volt *versus* SCE. The CVs were carried out at a potential scan rate of 200 mV s^{-1} at room temperature. The HOMO and LUMO energy levels (E_{HOMO} and E_{LUMO}) in electron volt (eV) were calculated according to the empirical equations (1) and (2):[1]

E_{HOMO} (eV) = -e (E_{onset} ox (V vs. SCE) + 4.74 V) *Eq(1)*

E_{LUMO} (eV) = -e (E_{onset} red (V vs. SCE) + 4.74 V) *Eq(2),*

and the energy gap value was obtained as follows: $E_g^{el} = (E_{LUMO} - E_{HOMO})$

The differences observed for the estimation of the energy gaps using experimental methods or theoretical calculations are well known. See for example: R. Stowasser, R. Hoffmann, *J. Am. Chem. Soc.* **1999**, *121*, 3414-3420.

[1] a) Y. Zhou, J. W. Kim, R. Nandhakumar, M. J. Kim, E. Cho, Y. S. Kim, Y. H. Jang, C. Lee, S. Han, K. M. Kim, J.-J. Kim, J. Yoon, *Chem. Commun.* **2010**, *46*, 6512-6514 and references therein; b) G. V. Loukova, *Chem. Phys. Lett.* **2002**, *353*, 244–252.

Table S16. Results of the emission decay measurements of the complexes in CH_2Cl_2. Luminescence decay times (τ_i) with their respective fractions of intensity (f_i) and normalized pre-exponential factor (a_i), defined by the multiexponential analysis of the decay curves: $I_F(t) = \Sigma a_i \times \exp(-t/\tau_i)$ and $f_i = a_i \times \tau_i / (\Sigma a_j \times \tau_j)$. Excitation wavelength: 380 nm.

	τ_i (ns)	f_i	a_i
ReL3	τ_1 = 3.9	0.004	0.1
	τ_2 = 100	0.996	0.9
ReL4	τ_1 = 3.7	0.01	0.13
	τ_2 = 80	0.99	0.87
ReL1[a]	τ_1 = 3.7	0.03	--
	τ_2 = 75	0.97	--

a: From ref. [8]

Table S17. Spectroscopic data of the complexes in acetonitrile and methanol. Maximum absorption wavelength (λ_{abs}), maximum phosphorescence and photoluminescence wavelengths (λ_P and λ_{PL}) and phosphorescence quantum yields (Φ_P). For solutions, complex concentration ~3.5 × 10^{-5} M, λ_{ex} = 380 nm. Undegassed solutions. *a* = Data from ref. [8].

Compounds	Acetonitrile			Methanol		
	λ_{abs} (nm)	λ_P (nm)	Φ_P	λ_{abs} (nm)	λ_P (nm)	Φ_P
ReL1[a]	299, 364	624	0.010	299, 362	623	0.006
ReL3	305, 364	626	0.010	302, 357	620	0.006
ReL4	302, 366	629	0.010	304, 360	618	0.007

Table S18. Results of the emission decay measurements of the complexes in the solid state (pristine powder). Luminescence decay times (τ_i) with their respective fractions of intensity (f_i) and normalized pre-exponential factor (a_i), defined by the multiexponential analysis of the decay curves: $I_F(t) = \Sigma a_i \times \exp(-t/\tau_i)$ and $f_i = a_i \times \tau_i / (\Sigma a_j \times \tau_j)$.

	τ_i (ns)	f_i	a_i
ReL3 [a]	τ_1 = 890 ± 20	0.05	0.44
	τ_2 = 185 ± 8	0.19	0.31
	τ_3 = 33 ± 2	0.76	0.26
ReL4 [b]	τ_1 = 563 ± 18	0.85	0.29
	τ_2 = 93 ± 10	0.12	0.26
	τ_3 = 12 ± 4	0.03	0.45
ReL1 [c]	τ_1 = 3.75	0.03	--
	τ_2 = 28.1	0.02	--
	τ_3 = 338	0.95	--

a: λ_{ex} = 420 nm, λ_{em} = 538-542 nm

b: λ_{ex} = 380 nm, λ_{em} = 538-542 nm

c: From ref. [8]. λ_{ex} = 380 nm, λ_{em} = 610-690 nm.

Figures

Crystallography

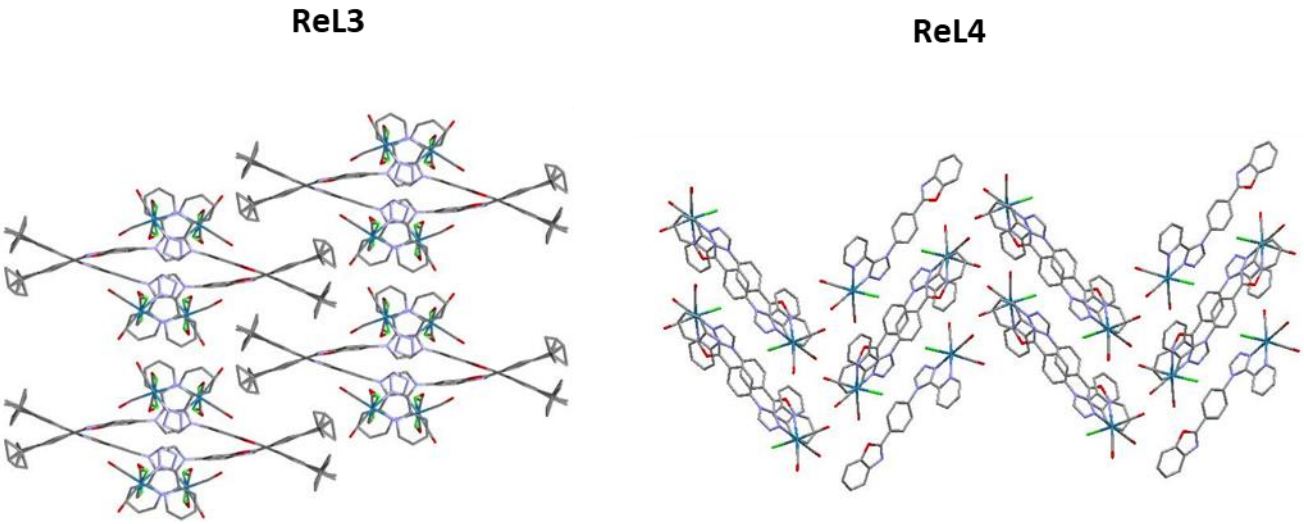

Figure S1. Crystal packing, view along *a* (**ReL3**) and *b* (**ReL4**).

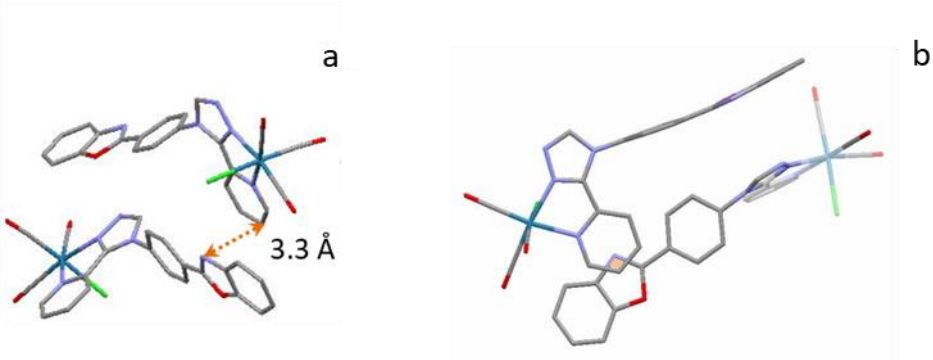

Figure S2. a) Orientation of two neighbouring molecules in the crystal cell of **ReL4**. b) Plan view of these molecules. The orange color indicates the overlap of the aromatic systems. Hydrogen atoms not represented for the sake of clarity.

TD-DFT calculations

ReL3		ReL4	
L + 5 (–0.71 eV)	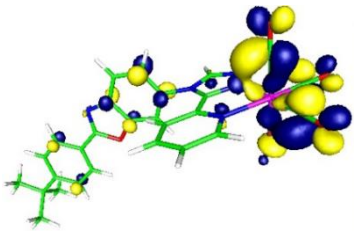	**L + 5** (–0.72 eV)	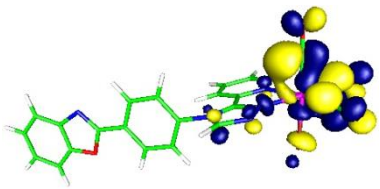
L + 4 (–0.81 eV)	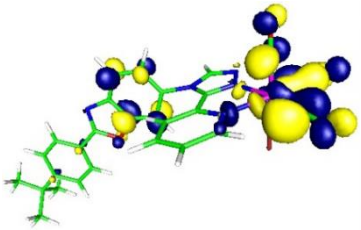	**L + 4** (–0.83 eV)	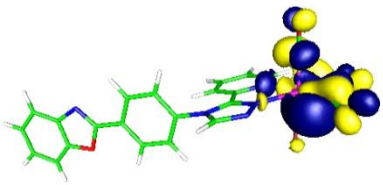
L + 3 (–0.85 eV)	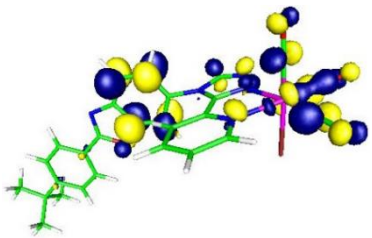	**L + 3** (–1.14 eV)	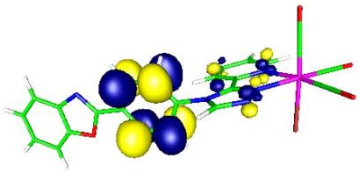
L + 2 (–1.63 eV)	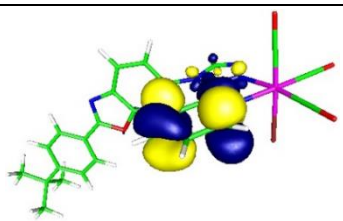	**L + 2** (–1.66 eV)	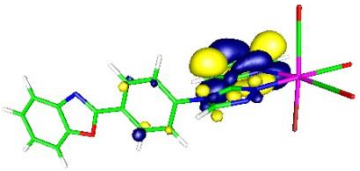
L + 1 (–2.05 eV)	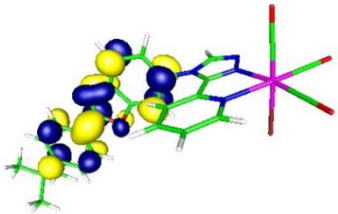	**L + 1** (–2.23 eV)	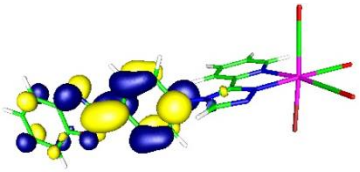
LUMO (–2.52 eV)	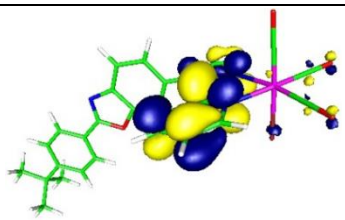	**LUMO** (–2.54 eV)	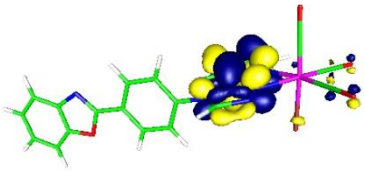

Figure S3. Isodensity plots of the frontier molecular orbitals of complexes **ReL3** and **ReL4** in CH_2Cl_2: Unoccupied orbitals.

ReL3		ReL4	
HOMO (–6.59 eV)	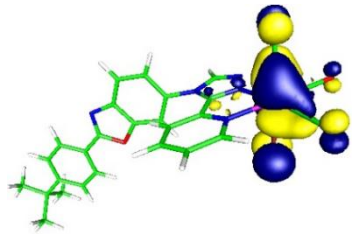	**HOMO** (–6.60 eV)	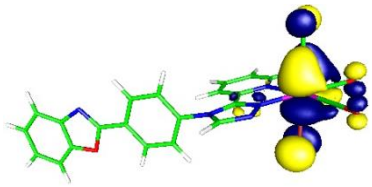
H – 1 (–6.71 eV)	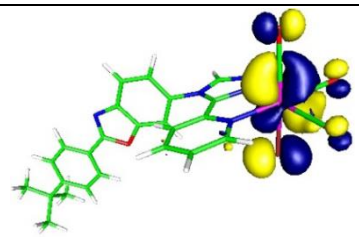	**H – 1** (–6.72 eV)	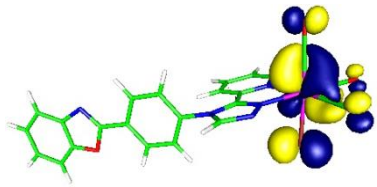
H – 2 (–6.87 eV)	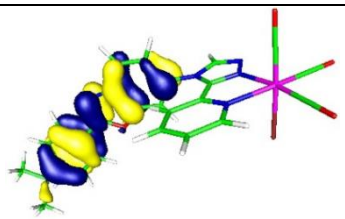	**H – 2** (–6.93 eV)	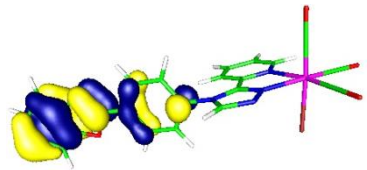
H – 3 (–7.15 eV)	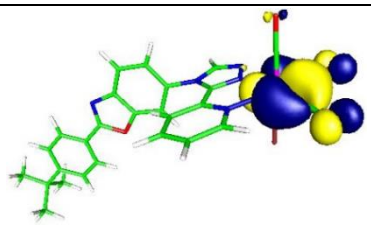	**H – 3** (–7.16 eV)	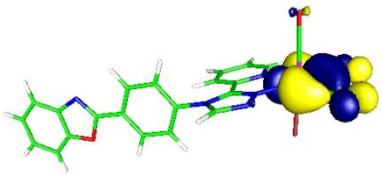
H – 4 (–7.66 eV)	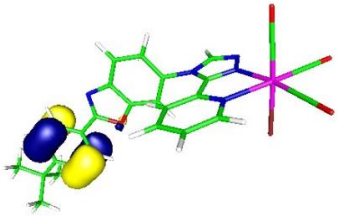	**H – 4** (–7.44 eV)	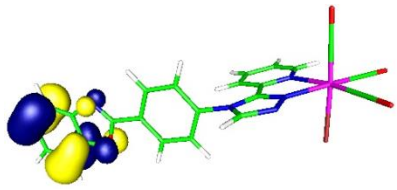
H – 5 (–7.81 eV)	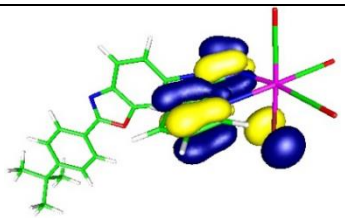	**H – 5** (–7.82 eV)	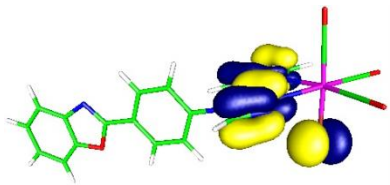

Figure S4. Isodensity plots of the frontier molecular orbitals of complexes **ReL3** and **ReL4** in CH_2Cl_2: Occupied orbitals.

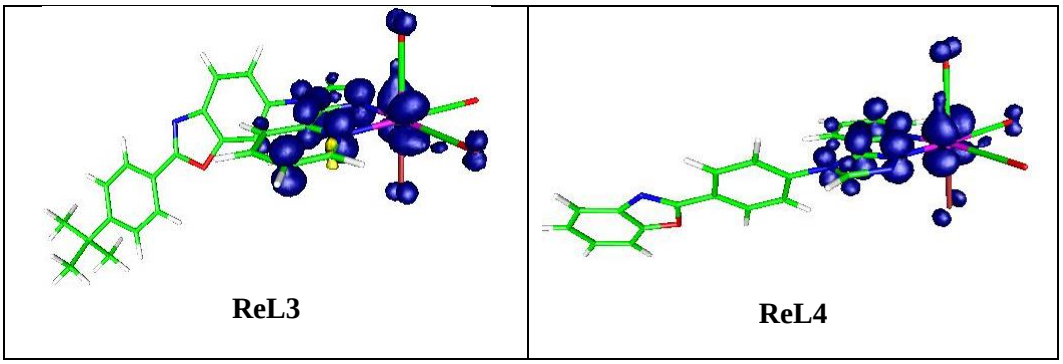

Figure S5. Spin density distribution for the lowest triplet state T_1 of complexes **ReL3** and **ReL4** in CH_2Cl_2. Calculations based on the optimized triplet state with DFT method at the PBE1PBE/LanL2DZ level.

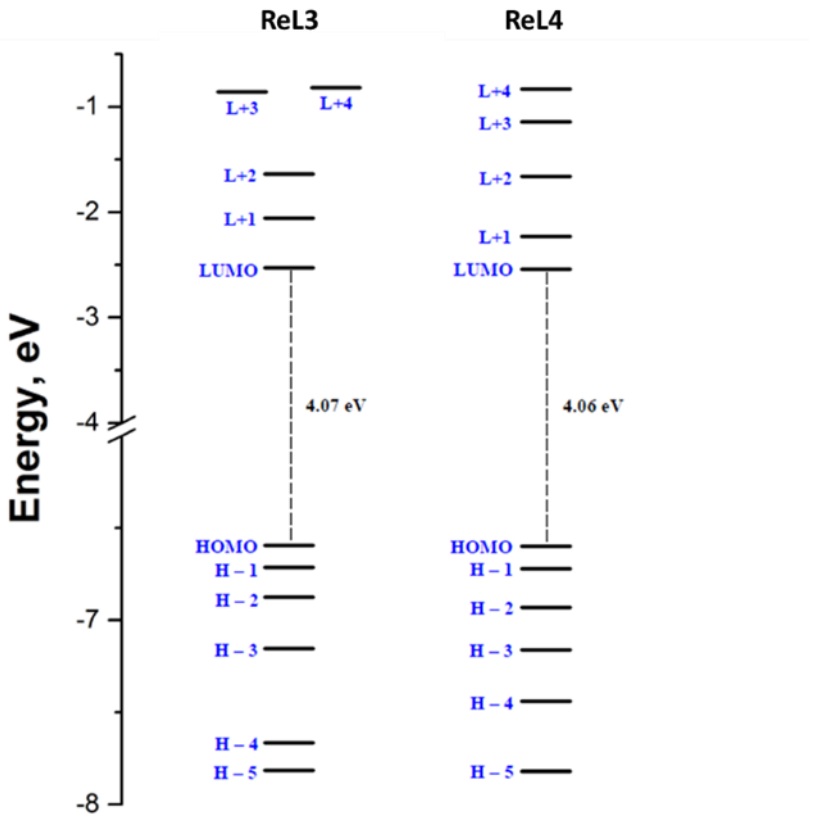

Figure S6. Molecular orbital diagrams of **ReL3** and **ReL4**.

Electrochemical selected curves

OSWV study was performed on a Pt working electrode in CH_2Cl_2 + 0.1 M *n*[Bu_4N][BF_4] at room temperature in the presence of ferrocene used as internal reference. Frequency 20 Hz, amplitude 20 mV, step potential 5 mV.
Cyclic voltammograms of the indicated compounds on a Pt working electrode in CH_2Cl_2 + 0.1 M *n*[Bu_4N][BF_4] at room temperature at a scan rate of 0.2 Vs^{-1} or at other mentioned scan rates.

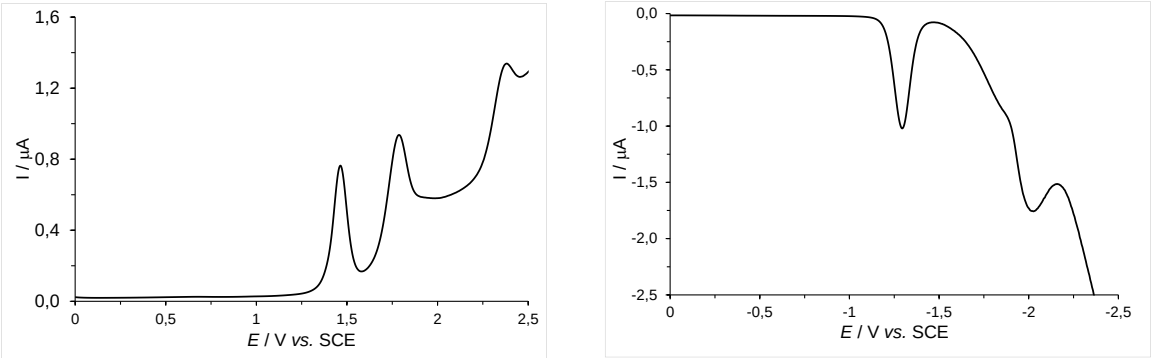

Figure S7. OSWV: anodic (left) and cathodic (right) scans of complex **ReL3**.

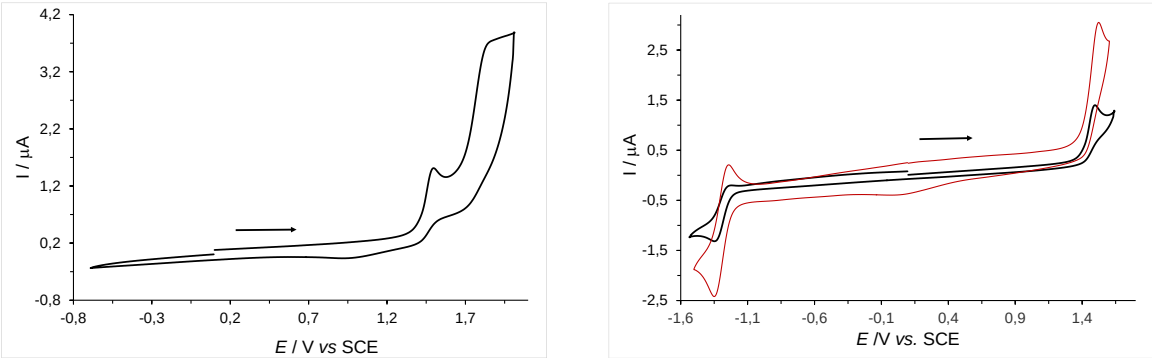

Figure S8. Segmented cyclic voltammograms of complex **ReL3**, in oxidation part at 0.2 V/s (left), and of the first oxidation and reduction processes at respectively, 0.2 (black), and 1.0 V/s (red) (right).

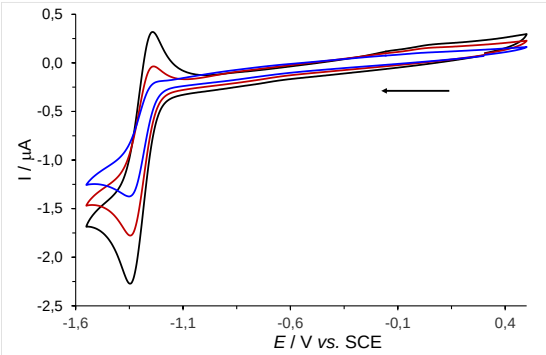

Figure S9. Cyclic voltammograms of the first reduction process of **ReL3** at respectively, 0.2 (blue), 0.5 (red), and 1.0 (black) V/s.

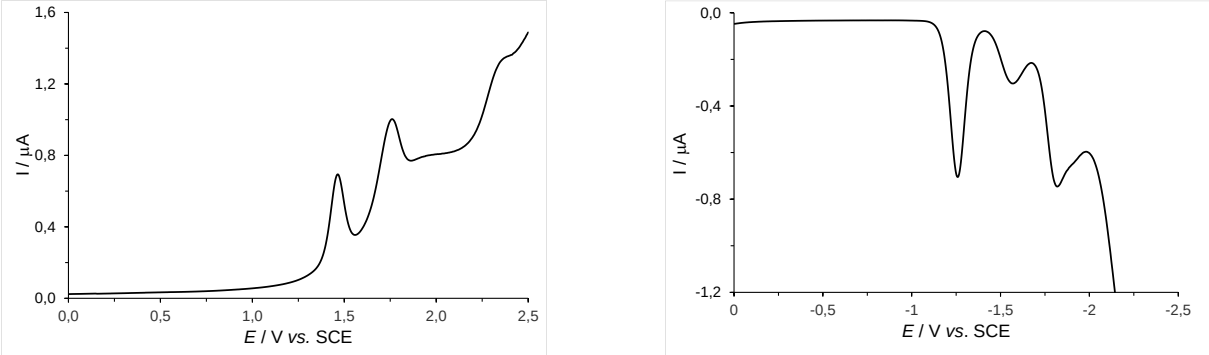

Figure S10. OSWV: anodic (left) and cathodic (right) scans of ligand **ReL4**.

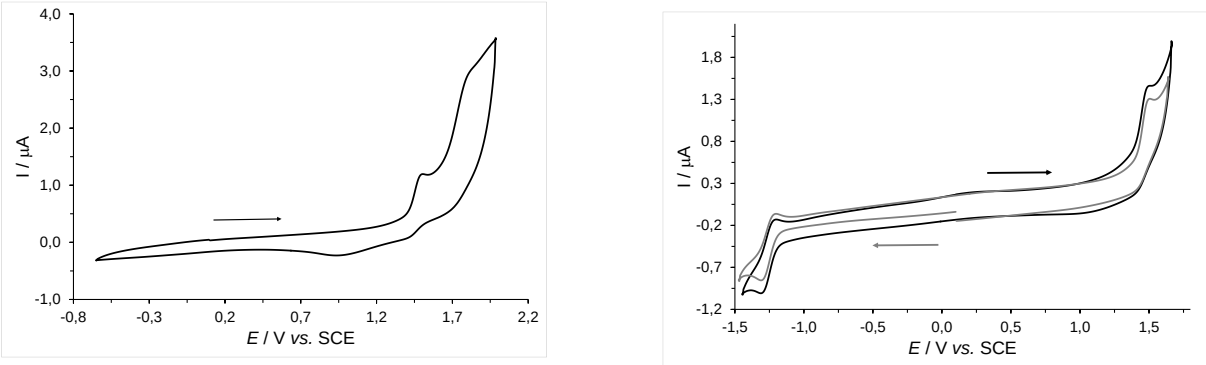

Figure S11. Segmented cyclic voltammograms of ligand **ReL4,** in oxidation part (left), and of the first oxidation and reduction processes scanning in the two different directions at 0.2 V/s (right).

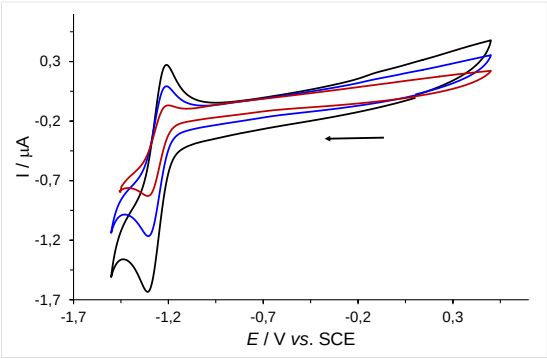

Figure S12. Cyclic voltammograms of the first reduction process of **ReL4** at, respectively, 0.2 (red), 0.5 (blue), and 1.0 (black) V/s.

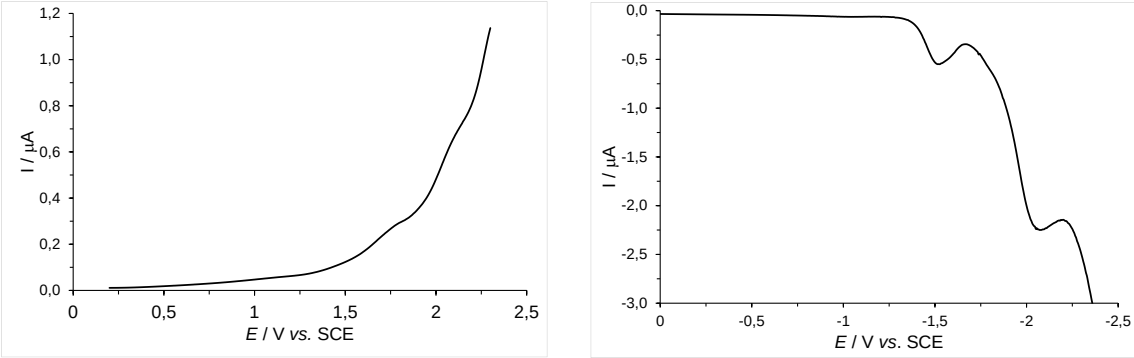

Figure S13. OSWV: anodic (left) and cathodic (right) scans of ligand **L3**.

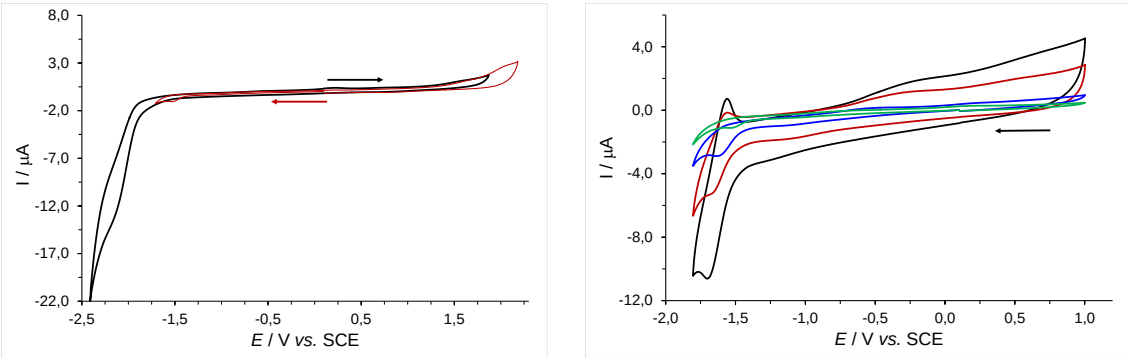

Figure S14. Cyclic voltammograms of ligand **L3** at 0.2 V/s toward anodic (black) and cathodic potential (left), and of its first reduction process at respectively, 0.2 (green), 1.0 (blue), 10.0 (red), and 20.0 (black) V/s (right).

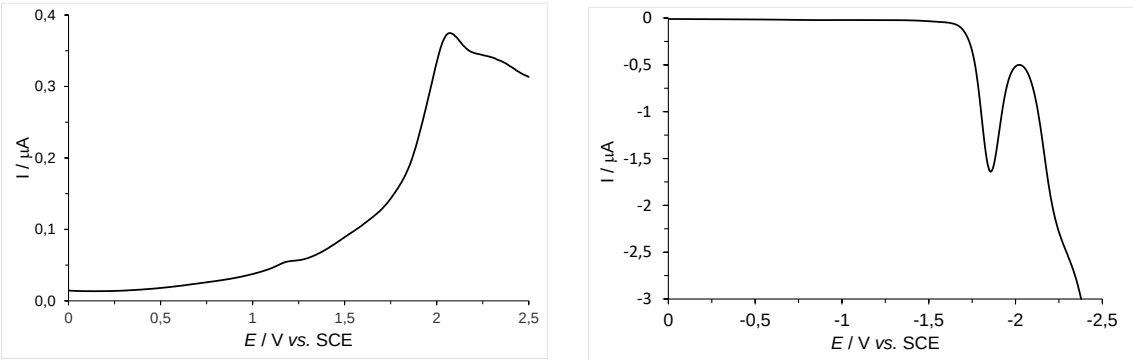

Figure S15. OSWV anodic (left) and cathodic (right) scans of ligand **L4**.

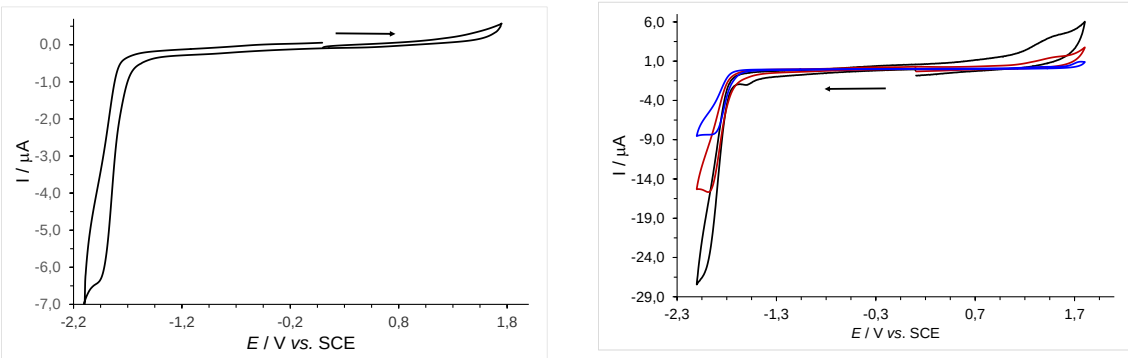

Figure S16. Cyclic voltammograms of ligand **L4** at 0.2 V/s (left), and at respectively, 0.1 (blue), 1.0 (red), and 5.0 (black) V/s (right).

Spectroscopy

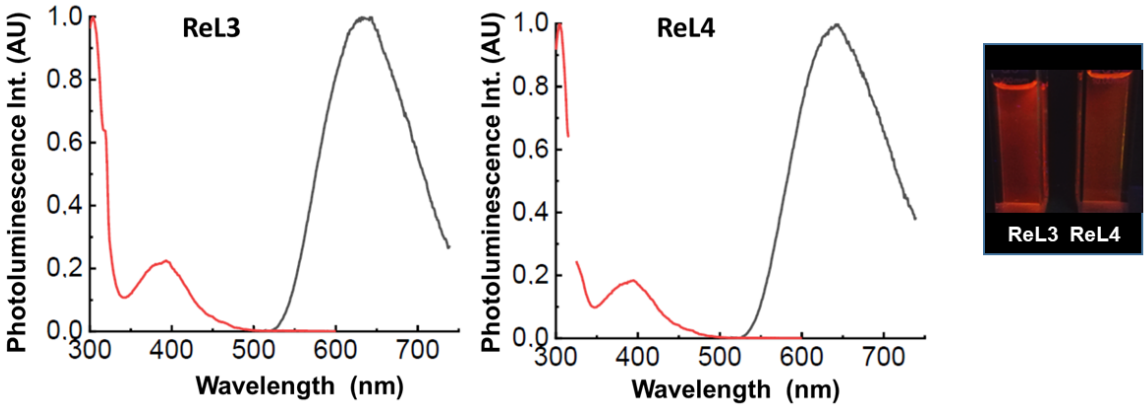

Figure S17. Left: Normalized excitation (λ_{em} = 640 nm) and emission (λ_{ex} = 380 nm) spectra of complexes **ReL3** and **ReL4** in CH_2Cl_2 at around 3.5 ×10^{-5} M. Right: corresponding samples illuminated by a hand-held UV lamp (365 nm).

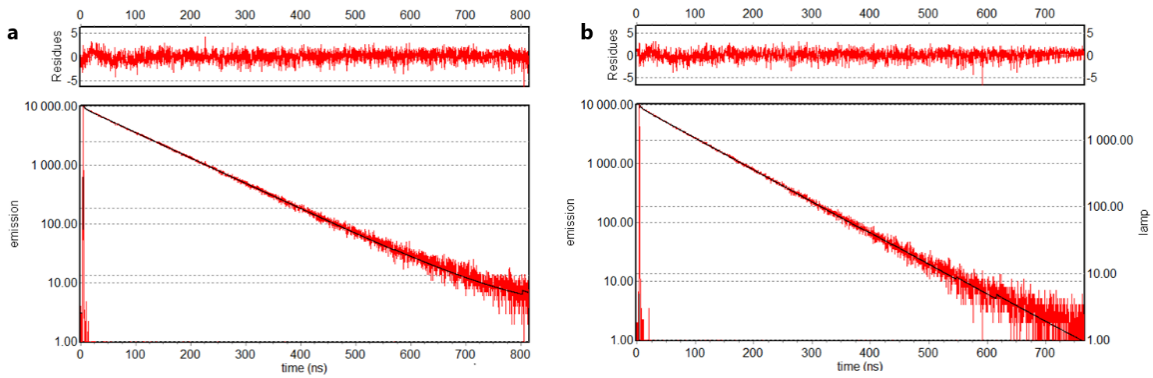

Figure S18. Photoluminescence decay curves of a) **ReL3** and b) **ReL4** in CH_2Cl_2. λ_{ex} = 380 nm; λ_{em} =580-660 nm. Solutions were bubbled with Ar (5 mins) before measurement.

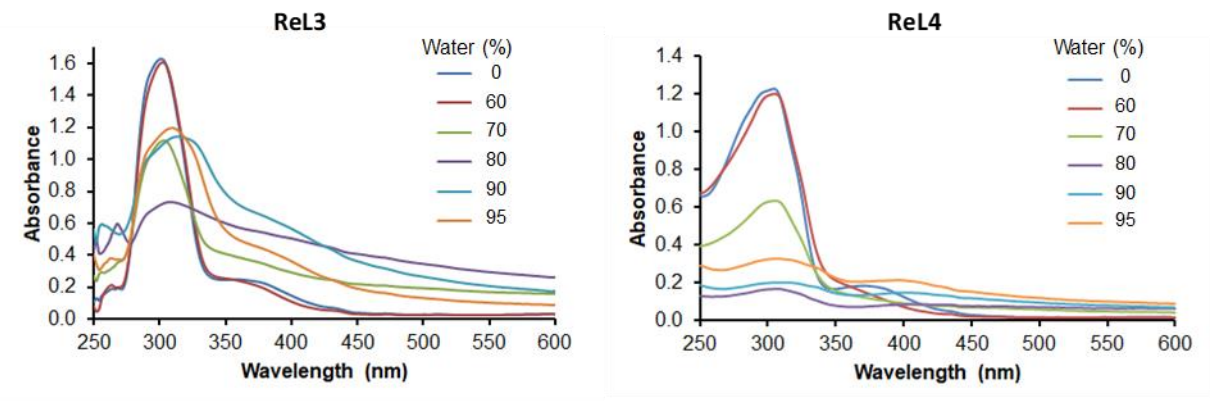

Figure S19. Absorption spectra of complexes **ReL3** (5.2 × 10^{-5} M) and **ReL4** (3.6 ×10^{-5} M) at constant concentration in water/acetonitrile mixtures.

Proton numbering

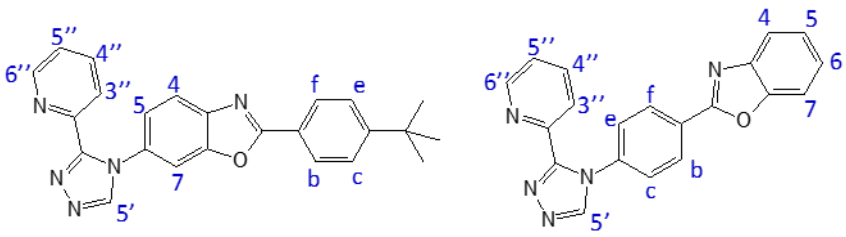

Figure S20. Proton numbering scheme for NMR. The numbering is the same for ligands and for complexes.